Atomic structure of screw dislocations intersecting the Au(111) surface: A combined scanning tunneling microscopy and molecular dynamics study

Engbæk, Jakob; Schiøtz, Jakob; Dahl-Madsen, Bjarke; Horch, Sebastian

Published in:
Physical Review B Condensed Matter

Link to article, DOI:
10.1103/PhysRevB.74.195434

Publication date:
2006

Document Version
Publisher's PDF, also known as Version of record

Atomic structure of screw dislocations intersecting the Au(111) surface: A combined scanning tunneling microscopy and molecular dynamics study

Jakob Engbæk and Jakob Schiøtz
Danish National Research Foundation's Center for Individual Nanoparticle Functionality (CINF), NanoDTU, Department of Physics, Technical University of Denmark, DK-2800 Kongens Lyngby, Denmark

Bjarke Dahl-Madsen and Sebastian Horch*
Center for Atomic-scale Materials Physics (CAMP), NanoDTU, Department of Physics, Technical University of Denmark, DK-2800 Kongens Lyngby, Denmark

(Received 27 July 2006; revised manuscript received 22 September 2006; published 27 November 2006)

The atomic-scale structure of naturally occurring screw dislocations intersecting a Au(111) surface has been investigated both experimentally by scanning tunneling microscopy (STM) and theoretically using molecular dynamics (MD) simulations. The step profiles of 166 dislocations were measured using STM. Many of them exhibit noninteger step-height plateaus with different widths. Clear evidence was found for the existence of two different populations at the surface with distinct (narrowed or widened) partial-splitting widths. All findings are fully confirmed by the MD simulations. The MD simulations extend the STM-, i.e., surface-, investigation to the subsurface region. Due to this additional insight, we can explain the different partial-splitting widths as the result of the interaction between the partial dislocations and the surface.

DOI: 10.1103/PhysRevB.74.195434 PACS number(s): 61.72.Ff, 68.37.Ef, 61.72.Bb, 68.35.Dv

I. INTRODUCTION

The material properties of metals and alloys are determined by the presence and structure of bulk defects like vacancies, impurities, dislocations, grain boundaries, and voids or microcracks. Dislocations are of particular interest, as they are the carriers of plastic deformation.

Dislocations at surfaces/interfaces affect many of the physical properties of the surfaces such as surface morphology.[1] They can also modify surface stress and thus influence other properties of surfaces such as chemical reactivity[2,3] or alloying properties.[4] Last but not least they play an important role in crystal growth[5] and have a huge potential to control the nucleation of small particles or thin films.[6–8]

In order to fully understand and control these properties, atomistic understanding of the entire dislocation structure is important, as the classic continuum methods fail to describe the structure of the dislocation cores. The scanning tunneling microscope (STM) is the instrument of choice when it comes to atomic resolution imaging of the structure and dynamics of surfaces and features on surfaces. There were several STM investigations about dislocations about a decade ago[9–16] but at that time interpretation of the results was difficult, largely because theorists could not yet perform the necessary large-scale calculations to understand the measurements.

In the meantime, progress in both theory and experiment leads to a renewed interest in investigating defects on the atomic scale. Especially the possibility to combine modern atomistic large scale simulations with STM observations (with down to atomic resolution at the surface) to provide detailed atomistic understanding of the structure and dynamics of defects, has triggered more recent investigations on naturally occurring and/or artificially introduced defects on single crystals[17–20] and thin films.[21]

In the present paper, we report on the atomic structure of naturally occurring screw dislocations intersecting a single crystal Au(111) surface, especially their partial-splitting width. The reason, why we chose this surface is that it exhibits the well-known herringbone reconstruction.[22,23] The reconstruction shows a large-scale ordered pattern that is mediated by long-range elastic lattice strain. A recent paper[24] has shown that the herringbone not only reacts to local stress variation, but is also sensitive to the overall surface stress. Already Barth *et al.*[22] speculated that the herringbone pattern might be used as a probe to elucidate the local distortion field in the vicinity of defects on the surface. This allows us, e.g., to find dislocations with a Burgers vector parallel to the surface. Such dislocations would otherwise be basically invisible in the STM.

II. PARTIAL SPLITTING OF DISLOCATIONS

A. Dislocations in fcc crystals

In fcc crystals, the vast majority of dislocations belong to the $\{111\}\langle 110\rangle$ slip system:[25,26] dislocations with Burgers vector $\mathbf{b}=\frac{1}{2}\langle 110\rangle$ gliding on $\{111\}$ planes. These dislocations split into partial dislocations according to the reaction $\mathbf{b}\rightarrow\mathbf{b_1}+\mathbf{b_2}$, where $\mathbf{b_1}=\frac{1}{6}\langle 211\rangle$ and $\mathbf{b_2}=\frac{1}{6}\langle 12\bar{1}\rangle$, or any other matching combination of $\frac{1}{6}\langle 112\rangle$ vectors. The two *partial dislocations* are separated by a planar fault in the crystal, an intrinsic stacking fault. The two partials repel each other due to their elastic interaction. The equilibrium distance between the dislocations is then given by a balance between the repulsion of the partial dislocations and the energy of the stacking-fault ribbon between them, the latter giving rise to an effective attractive force.

As the extension of this partial splitting is a function of the intrinsic stacking-fault energy,[25,26] the fcc group-11 met-

TABLE I. Literature values for intrinsic stacking-fault energies for fcc group-11 metals, in [mJ m^{-2}].

	Theoretical	Experimental
Cu	40–64[25,27–29]	41–78[28,29]
Ag	18–34[25,27,29]	15–22[28,29]
Au	45–59[27–29]	29–50[28,29]

als (Cu, Ag, Au) with their low intrinsic stacking-fault energy (i.e., large partial-splitting width) are most promising for this kind of investigation.

Literature values for intrinsic stacking-fault energies for fcc group-11 metals are shown in Table I (these values are still being debated, see, e.g., Ref. 30). According to *isotropic* elasticity theory,[25] the partial-splitting width (the width of the bulk stacking-fault ribbons) for Cu and Ag screw dislocations are about five to seven times the lattice constant, whereas for Au the width is around two lattice constants. This does, however, underestimate the splitting width, as these metals are far from isotropic.[31] For edge dislocations, the partial-splitting width is approximately a factor of 2 larger than for screw dislocations.

Experimentally, this has been verified by, e.g., weak-beam TEM measurements,[32,33] where the partial-splitting widths of Cu, Ag, and Au were measured as function of the dislocation orientation in bulk. It was found that the angle, under which the dislocation orients itself relative to the Burgers vector, has a large effect on the partial-splitting width. In general, Ag has the largest splitting widths (35–85 Å) compared to Cu and Au (both 20–45 Å). Screw dislocations have much smaller splitting widths than edge dislocations. The authors were unfortunately not able to find any perfect screw dislocation, but by extrapolating their data, they found that a pure screw dislocation in Ag should have a splitting width of about 20 Å, whereas in Cu and Au the value is reduced to about 10 Å.

B. Dislocations at fcc surfaces

Dislocations near surfaces can lower their energy by being perpendicular to the surface. At a (111) surface, dislocations with $\mathbf{b}=\frac{1}{2}[110]$ will orient as screw dislocations near the surface although this does not give the shortest line vector, whereas dislocations with $\mathbf{b}=\frac{1}{2}[\bar{1}10]$ or equivalent will stand as perpendicular to the surface as the {111} glide plane permits, and thus be a perfect edge dislocation.[19]

When a dislocation intersects a surface, its splitting width may be significantly altered.[19,31] Near the surface the partial dislocations no longer have to be parallel, and may re-orient in more screw-like directions (cf. Fig. 1), lowering the line energy at the expense of either increasing the stacking-fault area (if the lines move away from each other) or the interaction energy (if they move toward each other).

In the following, we shall only regard dislocations intersecting fcc(111) surfaces. Depending on the orientation of the partials with respect to each other, when approaching the surface, the dislocation's partial-splitting width either decreases (the partials point toward each other) or increases (the partials point away from each other) as compared to the bulk value. One therefore expects to find two different populations at the surface with distinct (narrowed or widened) partial-splitting widths. These partial-splitting widths can be assessed, if the stacking-fault width can be measured.

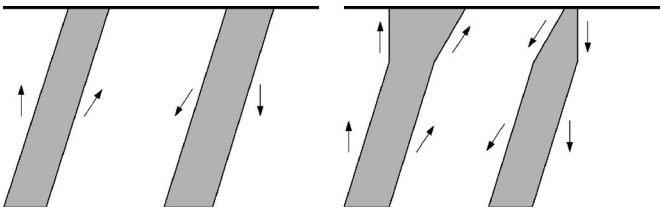

FIG. 1. Schematic view of the interaction of a surface (top line) with different types of dislocations, each represented by the stacking-fault ribbon (gray) with two Burgers vectors indicating the partial dislocations' orientation. Left: Original configuration without interaction. Right: Due to interaction with the surface, the partial dislocations rotate to align themselves with the Burgers vectors, i.e., toward a more screw-like orientation, thus reducing the line energy. This can lead to a widened (left) or a narrowed (right) partial-splitting width at the surface.

In the simplest case of pure edge dislocations, i.e., Burgers vector parallel to the surface, this is easily visible: By symmetry, the atoms of the stacking-fault ribbon are either displaced out of or into the surface. This gives rise to an isolated step segment on the surface with a fractional height of either $+1/3$ or $-1/3$ of the full step height at the end of the dislocation. The length of this fractional-height step segment is then a measure for the partial-splitting width.

For screw dislocations, with the Burgers vector almost perpendicular to the surface, the situation is slightly more complicated: Now the stacking-fault atoms can be displaced either 1/3 or 2/3 of a full step height out of the surface. Furthermore, from this fractional-height step segment a full-height step runs onto the surface. It is actually this single-ended ("disappearing") step that is widely considered as the characteristic footprint of a screw dislocation. Again, the length of the fractional-height step segment is a measure for the partial-splitting width.

As should have become clear from the above discussion, the atomic-scale step-profile structure contains information both about the bulk structure of the dislocation and about the dislocation-surface interaction. To fully understand these, we combine STM measurements of the step profiles (mostly step-height information) with atomistic simulations. We thus gain insight into the immediate subsurface region where the dislocation interacts with the surface.

III. EXPERIMENTAL PROCEDURE

A. Experimental setup

The experiments were performed in a standard ultrahigh vacuum (UHV) chamber, with base pressure below 5×10^{-11} mbar, equipped with a variable-temperature Århus-type scanning tunneling microscope (STM).[34] STM images were recorded at room temperature with as many

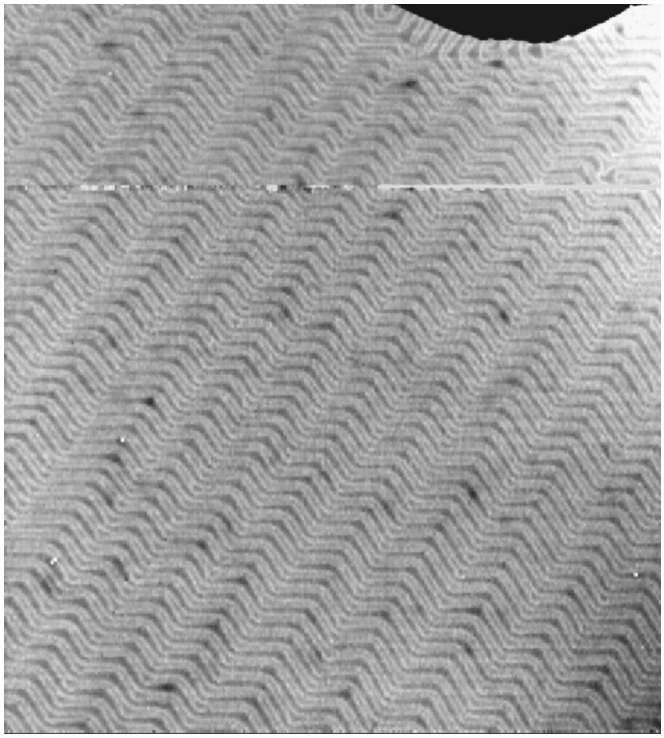

FIG. 2. Larger-scale STM image of a single large terrace with herringbone reconstruction on the clean Au(111). In the top part, a monoatomic step can be seen (the lower terrace appears black). Note how the herringbone pattern aligns perpendicular to the step (2700 Å × 3000 Å).

pixels per images as possible (typically 512 × 512) to get a sufficient lateral resolution in the step profiles.

The single crystal Au(111) surface is cleaned by cycles of sputtering with 3 kV Ar ions followed by annealing to 900 K. The final cleanliness of the crystal is checked with the STM. Even minute contaminations that would not be visible in, e.g., Auger electron spectroscopy can be detected by the STM, as the herringbone reconstruction is extremely sensitive to contamination. So the presence of a well-ordered herringbone pattern (Fig. 2) was used as indication that the surface is clean.

B. How to find dislocations on a surface

Due to its unsurpassed resolution, STM is ideally suited to investigate the atomic structure of dislocations at surfaces. Its weak point is, however, that it is not well suited for *finding* dislocations: Typical dislocation densities intersecting the surfaces of well-annealed metal crystals are only of the order of 10^4–10^6 mm^{-2},[25] i.e., chances of finding a dislocation in a typical STM image of less than 1000 Å width are only minute. In order to find these few dislocations, we therefore have to start our search with large-scale low-lateral-resolution STM images and look for footprints of dislocations.

Some dislocations have very visible signatures in STM images: As discussed above, screw dislocations easily show up as an emerging (or disappearing) step even on larger STM images (cf. Fig. 3). Others have weaker footprints and can only be spotted after zooming in on smaller-scale images, e.g., edge dislocations show up as longer or shorter step segments, depending on whether their partial-splitting width widens or not (Fig. 4). Even others have no direct footprint, and can only be found indirectly, e.g., if they modify the

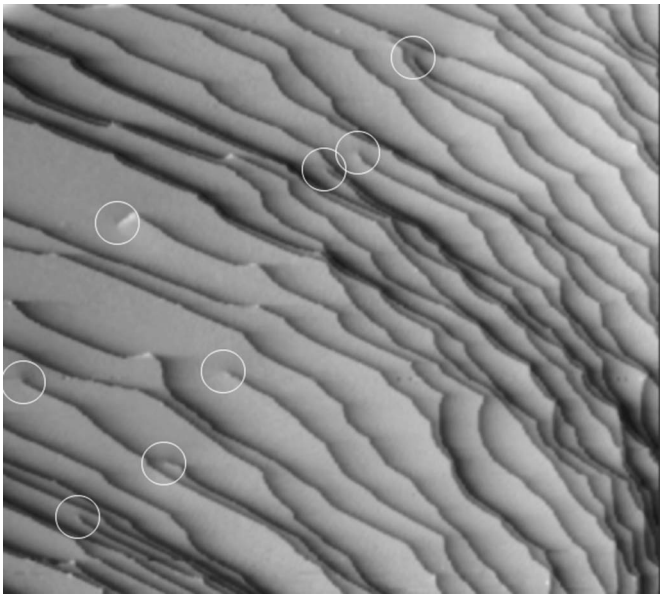

FIG. 3. Larger-scale STM image showing a family of eight screw dislocations (highlighted with circles). Screw dislocations are easily visible even at such low lateral resolution (here ca. 12 Å/pixel) since a surface step ends at the dislocation. The herringbone reconstruction or dislocations with less pronounced footprints are not visible under these conditions. Note that all dislocations in this family have the same turning sense (clockwise) (6000 Å × 5400 Å).

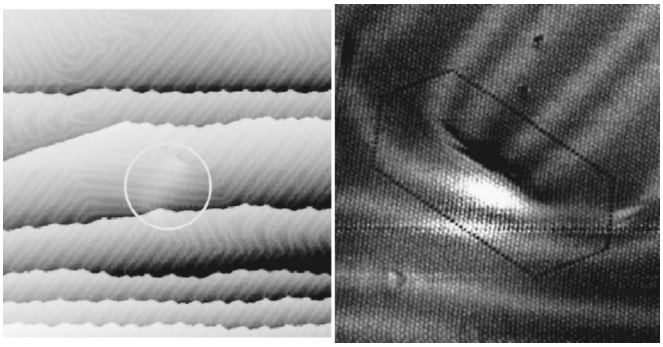

FIG. 4. Left: A step segment of 1/3 of a full step height on the central terrace indicates the presence of an edge dislocation with widened partial-splitting width (indicated by circle). It has been found due to the disturbance it causes in the herringbone pattern (1100 Å × 1100 Å). Right: Zoom in to atomic resolution. All atoms on a closed loop around the dislocation along a ⟨110⟩ path have been marked. There is one ⟨110⟩ vector less in the bottom line (39) than in the top line (40). Comparing to the larger-scale image (left), we believe that an intrinsic stacking fault extends to the lower left, visible as the brighter ribbon connecting to the next step. Analysis of the edge's step profile is complicated by the presence of two U-turn points of the herringbone (180 Å × 200 Å).

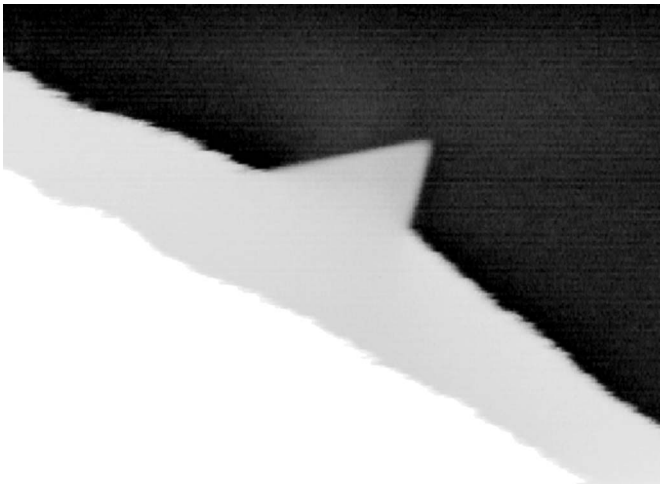

FIG. 5. Lomer-Cottrell lock pinning a step. Note that the step edges of the Lomer-Cottrell lock are not frizzy at all compared to the ordinary Au(111) steps (500 Å × 365 Å).

behavior of other surface features, like Lomer-Cottrell locks when pinning a step (Fig. 5). Dislocations without visible footprints, e.g., edges with narrowed partial-splitting width, are practically only found by chance or if they modify the herringbone, as any disturbance in its pattern reflects the presence of defects on the surface, as illustrated in Figs. 4 or 6.

Once spotted, we zoom in on the dislocation to obtain high-resolution images. In order to resolve partial splittings with our procedure described further down, we found it necessary to acquire images with a resolution of at least 1 pixel/Å and a width of up to 500 Å; atomic resolution is, however, not necessary.

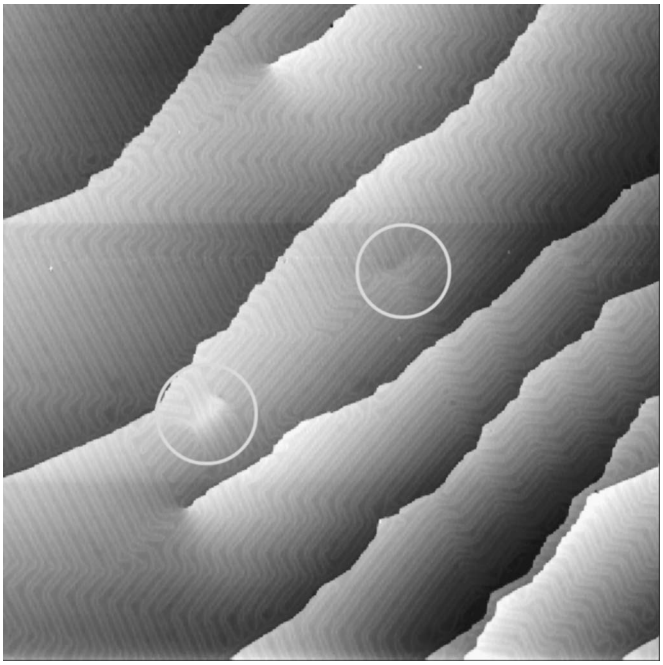

FIG. 6. Besides the two clearly visible screw dislocations, the modification of the herringbone pattern indicates the presence of at least three (more or less clearly visible) edge dislocations (indicated by circles) (3000 Å × 3000 Å).

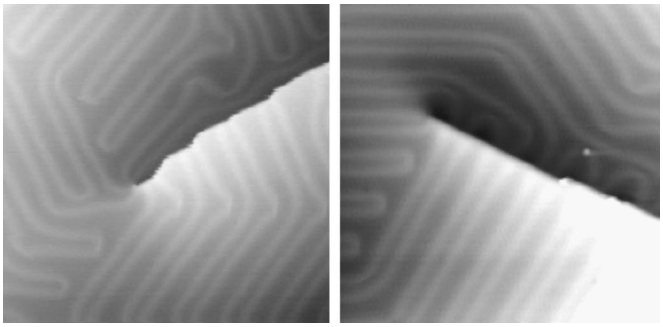

FIG. 7. Disturbed herringbone pattern in the vicinity of screw dislocations. Normally, the herringbone double lines do not end on a terrace. U-turns like those visible here are only seen close to defects (including steps) (Ref. 22) (500 Å × 480 Å).

Due to the difficulties in finding dislocations with weak footprints, we have until now mainly investigated screw dislocations, and here mainly those that are located on relatively large terraces, far away from steps. We have observed a lot of individual dislocations, but also some dislocation families (cf. Fig. 3), where all dislocations have similar properties, like turning sense (clockwise vs counterclockwise), what might be an indication of a common source for these families.

In general, we find that the herringbone pattern is influenced by the presence of dislocations (cf. Figs. 4, 6, and 7). From the known formation energies, we do not expect the herringbone to be able to influence the structure of dislocations, just the other way around. As it turns out, a computational analysis of this behavior is not feasible at the time being (due to the large unit cells needed). Therefore, we decided to concentrate on the investigation of the step profiles of the screw dislocations alone.

C. Step-profile extraction

The most important information one can extract from STM images of dislocations is the step height along the different step segments (the so-called "step profile"). This is, however, not a trivial task. Several methods have been proposed in the literature, yet most descriptions are quite vague.[10,11,19] Some authors even claim that step-profile extraction is not possible for frizzy steps, something we will show is not true.

There is one major problem when extracting step profiles from STM images: The surface under investigation is not perpendicular to the scanning tip. Thus the simplest approach of subtracting the heights of two lines running parallel to a step segment[10] might result in a wrong step height, depending on the tilt of the surface with respect to the tip. On dislocation-free surfaces, most STM software easily corrects for this tilt using a backplane subtraction. The surface around a screw dislocation is, however, inherently "screwed," thus making it impossible to remove the local tilt. A more advanced approach is therefore necessary.

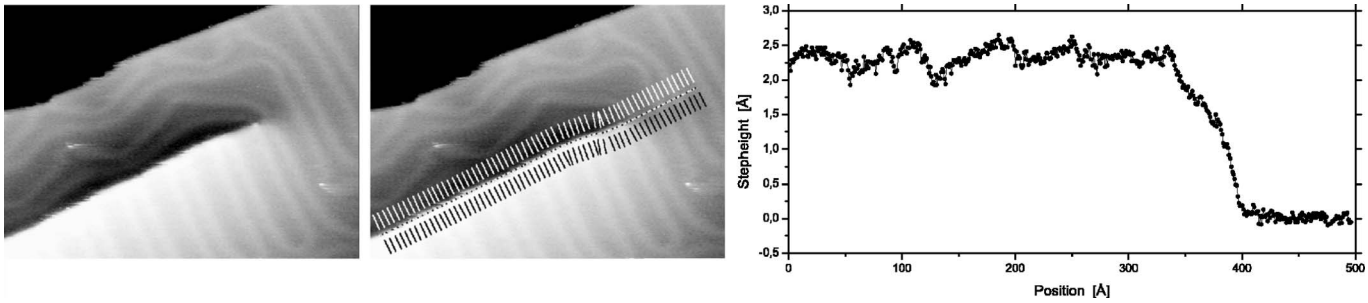

FIG. 8. Schematic explanation of step-profile extraction procedure. Left: Example of a screw dislocation (500 Å × 350 Å). The step disappears in the close-packed $[1\bar{1}0]$ direction. Note the herringbone double lines coming in perpendicular to the step on the upper terrace in $[11\bar{2}]$ direction and running parallel to the step on the lower terrace. Middle: First the user places straight segments along the step edge (dotted) and extending onto the terrace. Then the program calculates lines perpendicular to these segments (only some shown). Right: Resulting step-height profile for this dislocation. Note the wiggles due to the herringbone reconstruction. To analyze the plateau, one has to zoom in on the transition region.

To this end, we have developed a stable procedure (programmed using LabView/IMAQ), allowing us to extract reliable step profiles even for frizzy steps. As we found it hard to figure out how other authors have done this before, we shall here describe our extraction procedure in detail illustrated by Fig. 8.

In order to extract a step profile, the user first outlines the step using straight segments. On frizzy steps, we place these segments over the center of the frizzy parts. The last segment, reaching the point where the step vanishes into the surface, is normally extended onto the terrace to get a baseline as reference height (cf. Fig. 8 middle). The program then automatically places lines perpendicular to these segments with a spacing of about 1 Å (depending on image resolution) parallel to the segments. The starting distance of these lines from the segment and their lengths can be adjusted by the user. In order to analyze, e.g., frizzy steps, the lines may not come too close to the frizzy parts of the step. The program performs a linear regression of each individual line and extrapolates it onto the segment. The local step height of the segment is then calculated as the difference between the extrapolated line heights of the opposing lines on each side of the segment (resulting step profile, see Fig. 8 right). Using this procedure, even very frizzy steps can be analyzed up to full step height.

With this procedure, we automatically take care of local tilt and reduce line and pixel noise due to the linear regression (typical values for the line lengths we use are about 20–30 Å and for the distance from the segment to the line start ca. 10 Å). Another advantage of this approach is that even decorated steps can be analyzed, if the step decoration is narrower than the distance to where the lines start. This makes it possible to study, e.g., the influence of dislocations on the growth of thin films.

For further analysis, several parameters are extracted from each measured step profile (cf. Fig. 9):

(1) the "incline length," i.e., the horizontal distance from the end of the baseline to where the full step height is reached;

(2) the partial-splitting width (estimated to be situated in the middle of the two inclines around the plateau);

(3) the width of the plateau (if visible) where the step height is expected to be 1/3 or 2/3 of the full step height;

(4) the height of the baseline (as reference for the other heights);

(5) the height of the plateau;

(6) the full step height.

As will be discussed in Sec. V D, both height and length of the plateau might be obscured by the herringbone. In these cases, the incline length can be used to further analyze the dislocation. To make comparison to theory easier, this parameter has also been extracted from the simulated step profiles. Another problem is that the exact tip shape is unknown, making it impossible to deconvolute the step profiles to get the "real" widths of all parameters. All profiles presented in this paper are therefore raw-data profiles.

In general, the corrugation of the herringbone (about 0.2 Å or circa 10% of the full step height of 2.35 Å) is an additional complication encountered on the Au(111) surface. This perturbation shows up as a (not necessarily periodic) pattern on the step-height profile. We tried two ideas to reduce this perturbation: First, by adjusting the line length, one may be able to extend the lines such that they average over several herringbone lines; second, by changing the angle between the lines and the segments such that the lines run parallel with the herringbone lines. Most often, these approaches fail, as either the herringbone does not have the same angle to the step on both sides of the step (see, e.g., Figs. 7 or 8) or the surroundings of the dislocation do not allow for lines with the desired length or direction. The atomic corrugation, that can be as big as 0.1 Å, is, however, nicely averaged out by our algorithm and poses therefore no problem.

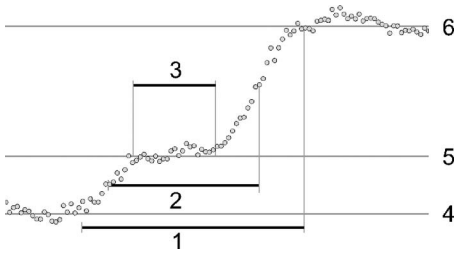

FIG. 9. The six parameters extracted from each step profile. See text for explanation.

IV. THEORETICAL METHODS

Molecular dynamics simulations were performed to help interpreting the observed step profiles. A block of Au crystal was set up in the computer, measuring 50 nm $\times$ 51 nm $\times$ 25 nm corresponding to 3.7 million atoms. The crystal was oriented with a [111] direction along the z axis, a $[11\bar{2}]$ direction along x, and a $[\bar{1}10]$ direction along the y axis. The herringbone reconstruction of the (111) surfaces was not included in the simulations. A screw dislocation with Burgers vector $\pm[110]$ was inserted between the two (111) surfaces, the dislocation was initially split up into two Shockley partial dislocations.

Where the dislocation intersects the surface, a step ends. This step can arrive at the dislocation from two different sides since the two partial dislocations are different: one has a Burgers vector perpendicular to the surface and results in a partial step of $\frac{2}{3}d_{111}$, the other has a Burgers vector with a large in-plane component, and results in a $\frac{1}{3}d_{111}$ step. The experimentally observed step profile will therefore consist of a small and a large partial step, and the ordering will depend on which partial dislocation the step meets first. In total, four different cases should be simulated, but as each simulation contains two surfaces on opposite sides of the slab, only two simulations are necessary.

Free boundary conditions were used in the simulations. In the z direction, this is desirable since a free surface is modeled. In the directions perpendicular to the free surface, periodic boundary conditions are impossible since the simulation cell contains a net Burgers vector. The atomic interactions were modeled using the effective medium potential,[35,36] with gold parameters fitted to reproduce the correct intrinsic stacking-fault energy.[37] Simulations were performed at a constant temperature of 300 K, using Langevin dynamics to keep the temperature constant.[38] The partial dislocations adjust their directions near the surface in such a way that they will either be tilted toward each other or away from each other at the surface, see Figs. 1 and 10

The dislocation quickly adjusts its splitting width, both in the bulk and near the surfaces. Unfortunately, the dislocation is attracted by the free surfaces, and will eventually start moving toward the edge of the simulation cell. This can be delayed by using a sufficiently large simulation cell. The cell should also be so large that the splitting width is not affected by the nearby free surfaces in the x and y directions. This was investigated in simulations performed at 0 K,[27] but this places a less strict requirement on the system size than the desire to prevent the dislocation from running out of the system. The step profile was taken while the dislocation was still reasonably close to the middle of the simulated system. Some thermal noise is seen in the step profile, this could only be avoided by averaging over a longer time, but such averaging is not possible due to the tendency of the dislocation to move.

V. RESULTS AND DISCUSSION

A. Total number of screw dislocations experimentally observed

Until now, we have found 166 dislocations. Compared to the other available STM investigations of dislocations, this number is huge. This may partially be due to the fact that we use a relatively new (not yet perfectly well annealed) Au crystal for our investigation, i.e., it might still have a slightly higher dislocation density, making it easier to spot dislocations.

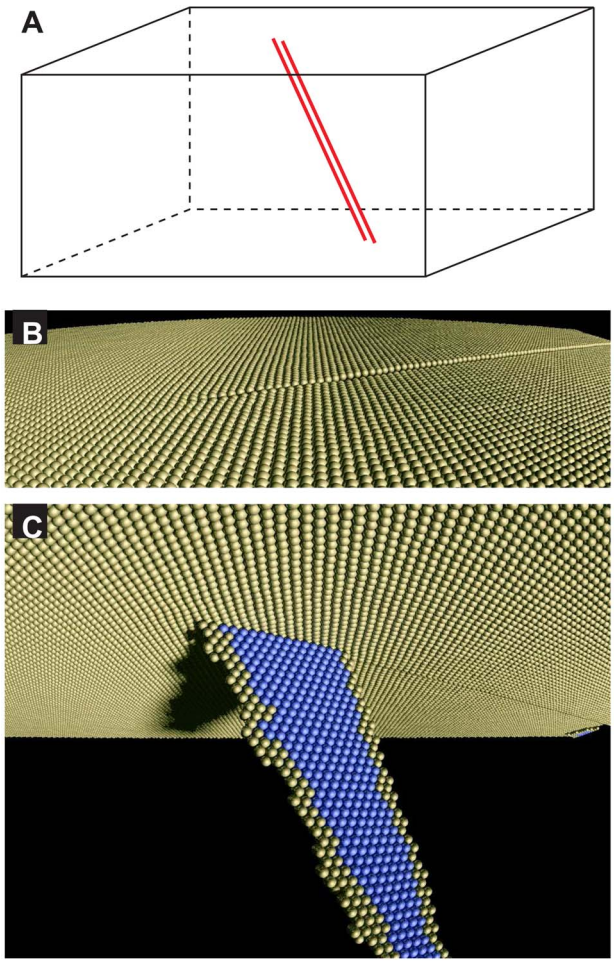

FIG. 10. (Color online) A: Sketch of the simulated system. The box is the block of atoms, the inserted partial dislocations are indicated in the middle. B: A step on the surface ends at the dislocation. C: The dislocation intersecting the surface, seen from below. Only atoms at the surface and in the dislocation core and stacking-fault ribbon are shown, all other atoms have been removed. The atoms in the stacking-fault ribbon have been colored. It is seen how the splitting width is enlarged near the surface. The partials are zigzagging slightly due to thermal fluctuations.

Still, even using the above-described analysis procedure, many dislocations cannot be step profiled. Most often, they are too close to other features, like other steps, so we cannot place long enough lines around the dislocation. All of them can, however, be analyzed with respect to their turning sense. In total, 62 dislocations were considered perfect enough to be step profiled.

B. Turning sense

The turning sense of the dislocation, i.e., whether the dislocation screw descends clockwise (CW) or counterclock-

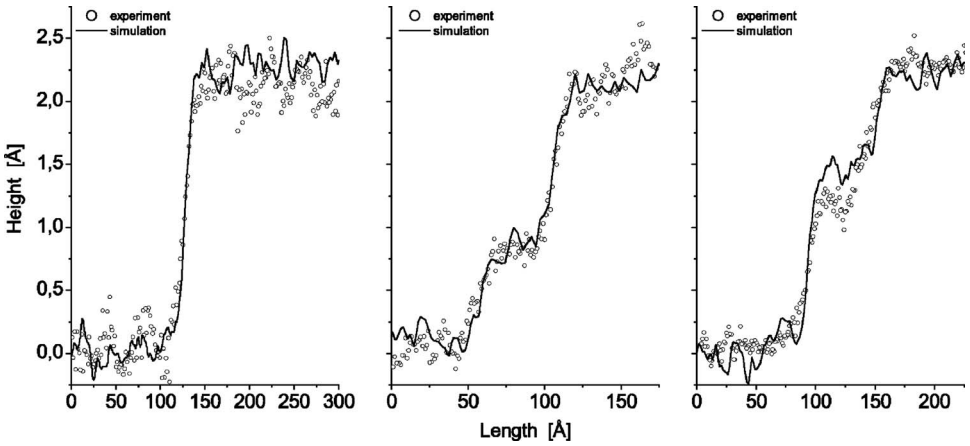

FIG. 11. Comparison of three simulated step profiles (full lines) with corresponding measured ones. Left: Narrowed partial-splitting width. Middle: Widened partial-splitting width, plateau at around 1/3 of full step height. Right: Widened partial-splitting width, plateau at around 2/3 of full step height.

wise (CCW) into the surface, can be determined for all observed dislocations. It should be randomly distributed. This matches our findings: Out of our 166 dislocations, 80 show CW and 86 CCW turning sense. Dislocations that come in families, however, very often possess the same turning sense (cf. Fig. 3), indicating that they stem from the same source. As it turns out, we see as many families with CW as with CCW turning sense, as should be expected.

C. Line scan comparison

In order to provide the reader with a feeling for how different step profiles look like, Fig. 11 shows simulated and measured step profiles for the three possible cases:

(1) narrowed partial-splitting width;

(2) widened partial-splitting width, plateau at around 1/3 of full step height;

(3) widened partial-splitting width, plateau at around 2/3 of full step height.

Already, screw dislocations in bulk Au have a relatively short partial-splitting width. As can be seen in the first line scan, it is therefore practically impossible to estimate the plateau length of the further narrowed dislocations at the surface as this drowns in the inherent width of the step decay into the surface. Note that this is true for both the experimental and the simulated line scans. For narrowed dislocations, we are therefore only able to give data on the incline length.

Besides being a nice confirmation that the simulations reproduce our measurements, these line scans clearly visualize the "noise" level we are dealing with in STM (mainly due to the herringbone). Remember that the herringbone is not included in the simulation of the gold screw dislocations.

D. Narrowed or widened partial-splitting width

There should be equally many narrowed and widened dislocations, as altering the Burgers vector or the glide plane causes the splitting width to change, and as there are two equally probable Burgers vectors and two equally probable (111) glide planes regardless of the Burgers vector.[27] As could be seen in the last section, the step profile of narrowed dislocations does not show a clear plateau. The presence or absence of a plateau was therefore used as a first means to distinguish these two groups of dislocations. There are 26 dislocations that show a clear plateau beyond doubt.

For the other dislocations, it is often the herringbone that makes it difficult to decide whether there is a plateau or not. A slightly different approach was therefore used in order to

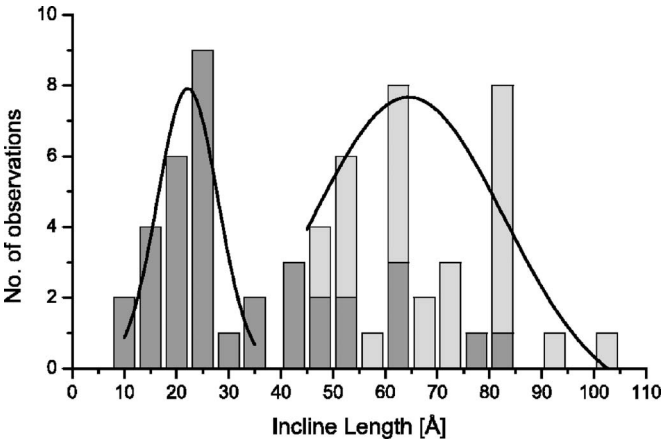

FIG. 12. Distribution of the incline lengths for narrowed (left part) and widened (right part) screw dislocations. Dislocations with clearly visible plateau have been colored in lighter gray. Gaussians have been added to guide the eye.

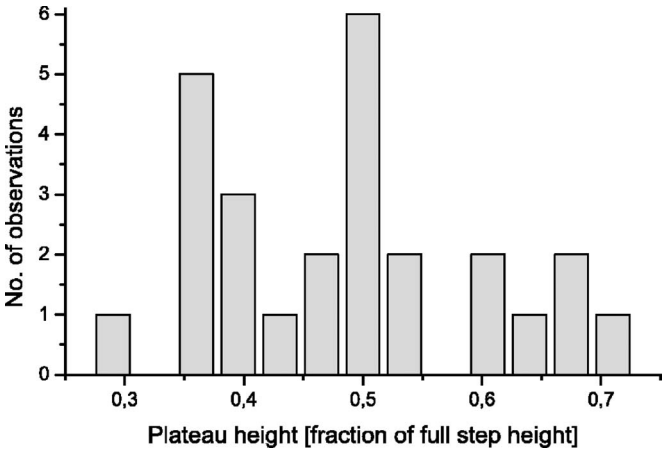

FIG. 13. Plateau height distribution for those widened dislocations that show a clear plateau (26 of the 38 widened dislocations).

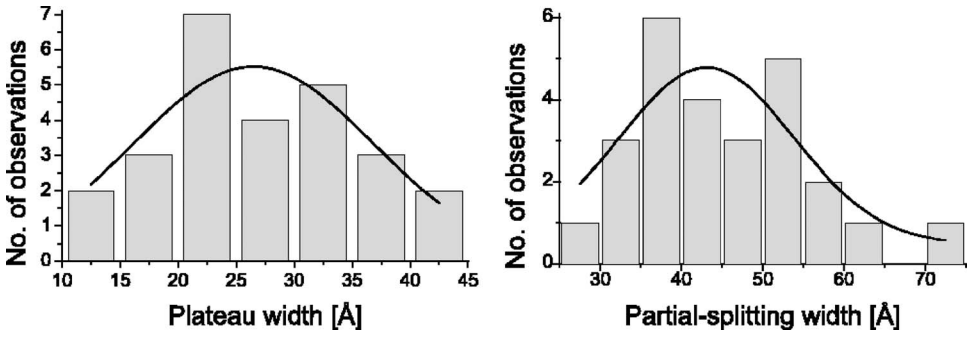

FIG. 14. Plateau width and partial-splitting width distributions for those widened dislocations that show a clear plateau (26 of the 38 widened dislocations).

find out whether a dislocation is narrowed or widened: Based on our total dataset, we decided that all dislocations showing an incline length of more than 35 Å should be considered widened. This leads to 24 narrowed dislocations and 38 widened ones. Fortunately, only 2 of our 62 dislocations are dubious and have incline lengths in the range of 35–45 Å, i.e., we do not know which group to assign them to. As a consequence of this problem, we decided to present in the following data not only for the partial-splitting width, but also for the incline length and compare both to the simulations.

1. Incline length

For each dislocation the incline length has been measured. The distribution for both groups is shown in Fig. 12. A Gaussian has been added to guide the eye. The mean incline length for the narrowed dislocations is 22 Å and 64 Å for the widened ones. The reason for the broad distribution is not only noise, but also uncertainties induced by the herringbone. Analysis of the simulated step profiles gives incline lengths of 19 Å for the narrowed and 67 Å for the widened dislocation, which compares nicely to the measured values.

From theory, we expect narrowed and widened dislocations to be equally probable. Indeed, our 24 to 38 ratio fits this picture nicely. It should be noted here that in recent work on Ag (111) (Ref. 19) only widened dislocation could be observed. As far as we know, our observations are, indeed, the first experimental observations of narrowed dislocations.

2. Plateau height

As discussed above, we expect the plateau height to be either 1/3 or 2/3 of a full step height. For obvious reasons, we can only analyze widened dislocations, where the plateau is observable. Figure 13 presents the measured plateau heights. Unfortunately, instead of two peaks at 1/3 and 2/3 our data look more like a peak at 1/3 and one at 1/2. It is plausible that the Herringbone is responsible for that smear out.

3. Plateau width and partial-splitting width

The plateau width and partial-splitting width could only be analyzed for those widened dislocations that show a clear plateau. Figure 14 shows the respective distributions. Once again there is a good agreement with the values extracted from the simulations: The theoretical value of the plateau width is 27 Å and the partial-splitting width is 45 Å, which compare nicely to the experimentally found average plateau width of 26 Å and partial-splitting width of 43 Å.

VI. CONCLUSION

The atomic-scale structure of screw dislocations intersecting a Au(111) surface has been investigated both experimentally by scanning tunneling microscopy and theoretically using nanoscale atomistic simulations. Three distinct properties of the dislocation cores were studied and found to be in good agreement with theory. For the first time, both widened and narrowed dislocations could be observed. First experimental evidence was found for two distinct partial-splitting widths of screw dislocations intersecting a surface. Atomic scale MD simulations fully confirmed these findings.

ACKNOWLEDGMENTS

The Center for Individual Nanoparticle Functionality (CINF) is sponsored by the Danish National Research Foundation.

*Electronic address: horch@fysik.dtu.dk

[1] E. Lundgren, B. Stanka, W. Koprolin, M. Schmid, and P. Varga, Surf. Sci. **423**, 357 (1999).
[2] J. de la Figuera, A. K. Schmid, and R. Q. Hwang, Surf. Sci. Lett. **415**, 993 (1998).
[3] J. de la Figuera, K. Pohl, A. K. Schmid, N. C. Bartelt, J. Hrbek, and R. Q. Hwang, Surf. Sci. **531**, 29 (2003).
[4] R. Q. Hwang and M. C. Bartelt, Chem. Rev. (Washington, D.C.) **97**, 1063 (1997).
[5] H. Brune, Surf. Sci. Rep. **31**, 121 (1998).
[6] D. D. Chambliss, R. J. Wilson, and S. Chiang, Phys. Rev. Lett. **66**, 1721 (1991).
[7] K. Pohl, M. C. Bartelt, J. de la Figuera, N. C. Bartelt, J. Hrbek, and R. Q. Hwang, Nature (London) **397**, 238 (1999).
[8] J. V. Lauritsen, M. Nyberg, R. T. Vang, M. V. Bollinger, B. S. Clausen, H. Topsøe, K. Jacobsen, E. Lægsgaard, J. K. Nørskov,

and F. Besenbacher, Nanotechnology **14**, 385 (2003).
[9] G. Cox, D. Szynka, U. Poppe, K. H. Graf, K. Urban, C. Kisielowski-Kemmerich, J. Kruger, and H. Alexander, Phys. Rev. Lett. **64**, 2402 (1990).
[10] A. Samsavar, E. S. Hirschorn, T. Miller, F. M. Leibsle, J. A. Eades, and T.-C. Chiang, Phys. Rev. Lett. **65**, 1607 (1990).
[11] J. F. Wolf and H. Ibach, Appl. Phys. A **A52**, 218 (1991).
[12] R. Stalder, H. Sirringhaus, N. Onda, and H. v. Kaenel, Surf. Sci. **258**, 153 (1991).
[13] G. O. Potschke and R. J. Behm, Phys. Rev. B **44**, 1442 (1991).
[14] M. Schmid, A. Biedermann, H. Stadler, and P. Varga, Phys. Rev. Lett. **69**, 925 (1992).
[15] H. Brune, H. Roder, C. Boragno, and K. Kern, Phys. Rev. B **49**, 2997 (1994).
[16] J. Jacobsen, L. P. Nielsen, F. Besenbacher, I. Stensgaard, E. Lægsgaard, T. Rasmussen, K. W. Jacobsen, and J. K. Nørskov, Phys. Rev. Lett. **75**, 489 (1995).
[17] J. de la Figuera, M. A. Gonzáles, R. García-Martínez, J. M. Rojo, O. S. Hernán, A. L. V. de Parga, and R. Miranda, Phys. Rev. B **58**, 1169 (1998).
[18] O. R. de la Fuente, J. A. Zimmerman, M. A. Gonzáles, J. de la Figuera, J. C. Hamilton, W. W. Pai, and J. M. Rojo, Phys. Rev. Lett. **88**, 036101 (2002).
[19] J. Christiansen, K. Morgenstern, J. Schiøtz, K. W. Jacobsen, K.-F. Braun, K.-H. Rieder, E. Lægsgaard, and F. Besenbacher, Phys. Rev. Lett. **88**, 206106 (2002).
[20] O. R. de la Fuente, M. A. Gonzáles, and J. M. Rojo, Philos. Mag. **83**, 485 (2003).
[21] J. de la Figuera, K. Pohl, O. R. de la Fuente, A. K. Schmid, N. C. Bartelt, C. B. Carter, and R. Q. Hwang, Phys. Rev. Lett. **86**, 3819 (2001).
[22] J. V. Barth, H. Brune, G. Ertl, and R. J. Behm, Phys. Rev. B **42**, 9307 (1990).
[23] H. Bulou and C. Goyhenex, Phys. Rev. B **65**, 045407 (2002).
[24] O. Schaff, A. K. Schmid, N. C. Bartelt, J. de la Figuera, and R. Q. Hwang, Mater. Sci. Eng., A **319**, 914 (2001).
[25] D. Hull and D. J. Bacon, *Introduction to Dislocations*, Vol. 37 of International Series on Material Science and Technology (Butterworth-Heinemann, Oxford, UK, 1984), 3rd ed.
[26] J. P. Hirth and J. Lothe, *Theory of Dislocations* (Wiley, New York, 1982).
[27] J. Christiansen, "Dislocations and interfaces," Ph.D. thesis, June 2003 (Technical University of Denmark, 2003).
[28] N. Bernstein and E. B. Tadmor, Phys. Rev. B **69**, 094116 (2004).
[29] N. M. Rosengaard and H. L. Skriver, Phys. Rev. B **47**, 12865 (1993).
[30] T. J. Balk and K. J. Hemker, Philos. Mag. A **81**, 1507 (2001).
[31] T. Rasmussen, K. W. Jacobsen, T. Leffers, and O. B. Pedersen, Phys. Rev. B **56**, 2977 (1997).
[32] D. J. H. Cockayne, M. L. Jenkins, and I. L. F. Ray, Philos. Mag. **24**, 1383 (1971).
[33] M. L. Jenkins, Philos. Mag. **26**, 747 (1972).
[34] E. Lægsgaard, F. Besenbacher, K. Mortensen, and I. Stensgaard, J. Microsc. **152**, 663 (1988).
[35] K. W. Jacobsen, J. K. Nørskov, and M. J. Puska, Phys. Rev. B **35**, 7423 (1987).
[36] K. W. Jacobsen, P. Stoltze, and J. K. Nørskov, Surf. Sci. **366**, 394 (1996).
[37] T. Rasmussen (private communication).
[38] M. P. Allen and D. J. Tildesley, *Computer Simulation of Liquids* (Claredon, Oxford, 1987).